Nano Res (2010) 3: 8–15
DOI 10.1007/s12274-010-1002-8
Research Article

Projected Performance Advantage of Multilayer Graphene Nanoribbons as a Transistor Channel Material

Yijian Ouyang[1] (✉), Hongjie Dai[2], and Jing Guo[1] (✉)

[1] Department of Electrical and Computer Engineering, University of Florida, Gainesville, FL 32611, USA
[2] Department of Chemistry, Stanford University, Stanford, CA 94305, USA

Received: 2 October 2009 / Revised: 13 November 2009 / Accepted: 15 November 2009
© The Author(s) 2010. This article is published with open access at Springerlink.com

ABSTRACT

The performance limits of a multilayer graphene nanoribbon (GNR) field-effect transistor (FET) are assessed and compared with those of a monolayer GNRFET and a carbon nanotube (CNT) FET. The results show that with a thin high dielectric constant (high-κ) gate insulator and reduced interlayer coupling, a multilayer GNRFET can significantly outperform its CNT counterpart with a similar gate and bandgap in terms of the ballistic on-current. In the presence of optical phonon scattering, which has a short mean free path in the graphene-derived nanostructures, the advantage of the multilayer GNRFET is even more significant. Simulation results indicate that multilayer GNRs with incommensurate non-AB stacking and weak interlayer coupling are the best candidates for high-performance GNRFETs.

KEYWORDS

graphene nanoribbon (GNR), multilayer graphene, new channel material, field-effect transistor, carbon nanotube (CNT)

Introduction

Graphene [1–3] is a monolayer of carbon atoms packed into a honeycomb lattice and possesses an atomically thin body and an area that is orders of magnitude greater, making it an ideal two-dimensional (2-D) system. A 2-D graphene is a semimetal without a bandgap, but a bandgap opens if a field-effect transistor (FET) channel is built on a nanometer-wide graphene nanoribbon (GNR) due to the width direction confinement [4]; this also results in subband formation [5]. The high mobility (up to 200 000 $cm^2/(V\cdot s)$) and carrier velocity (~10^8 cm/s) demonstrated in 2-D graphene have stimulated strong interests in graphene electronics [1]. The transport properties of GNRs in experiments have been so far hindered by imperfect edges [6, 7], but excellent transport properties have been theoretically predicted for structurally perfect GNRs [8]. A GNRFET, however, suffers from the problem of a low on-current due to its nanometer-wide channel, and it has been previously shown that the ballistic performance limits of a monolayer GNRFET are no better than a carbon nanotube (CNT) FET in terms of the on-current to on-off current ratio [9].

In this study we assess the performance limits of GNRFETs and CNTFETs using a well-established ballistic transistor model, which has previously been applied to various 2-D and 1-D channel transistors [10]. The performance limits of a transistor are achieved when the contacts are ideal and the channel is ballistic (i.e., no scattering). Schottky barriers can play an important role in CNTFETs [11] and GNRFETs.

Address correspondence to guoj@ufl.edu

The Schottky barrier is known to lower the on-current and increase the off-current due to ambipolar *I–V* characteristics. These detrimental effects in Schottky barrier CNTFETs, however, can be eliminated by using a metal-oxide-semiconductor (MOS) FET device structure [12], which has heavily doped source and drain extensions as shown in Fig. 1(a). The performance limits are therefore assessed for a ballistic MOSFET structure with semi-infinite source and drain extensions. Under these conditions, the simple semiclassical model agrees with detailed quantum mechanical transistor simulations for a channel length down to about 10 nm [10], as long as the direct source–drain tunneling current is relatively small compared to the total source–drain current.

Multilayer GNRs have been demonstrated in recent experiments [13, 14]. We show that the modeled ballistic performance limits of a multilayer GNRFET can be significantly better than the corresponding CNTFET in terms of the on-current to on-off current ratio. The advantage becomes even bigger in the presence of optical phonon (OP) scattering, which is known to be strong in graphene-derived nanostructures.

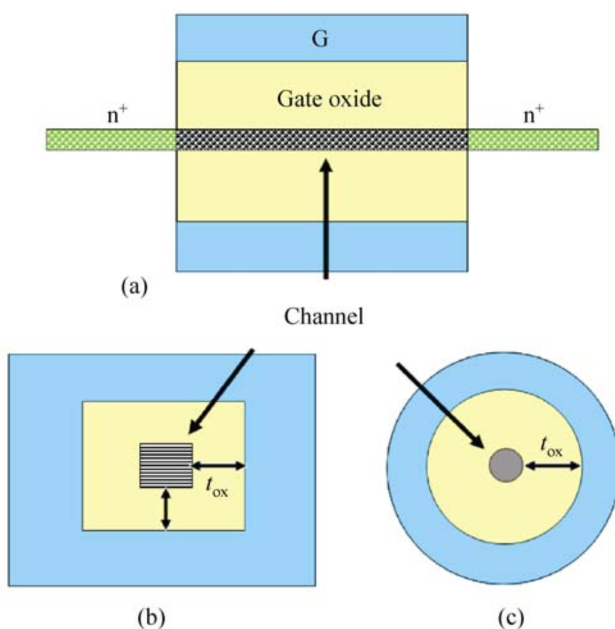

Figure 1 Schematic structure of the modeled multilayer GNRFET and CNTFET: (a) the MOSFET has an intrinsic channel and heavily doped source and drain extensions; (b) the cross section of the wrapped-around gate GNRFET; (c) the cross section of the CNTFET with a coaxial gate

The important role of gating technology and interlayer coupling are investigated in order to realise the performance advantage of multilayer GNRFETs over CNTFETs. We found that weak interlayer coupling, which is accessible through incommensurate non-AB stacking, is desired for a high-performance multilayer GNRFET.

1. Approach

To ensure a fair comparison, the modeled graphene nanoribbon and carbon nanotube have similar bandgaps. The (20, 0) zigzag CNT is semiconducting, which results in a diameter of $d_{CNT} \approx 1.6$ nm and a bandgap of $E_g \approx 0.50$ eV. The $n = 22$ armchair edge GNR (AGNR) (where n denotes the number of carbon dimer lines [15]) is also semiconducting, which results in a width of $W_{GNR} \approx 2.7$ nm and a bandgap of $E_g \approx 0.52$ eV for a monolayer GNR. Both transistors have doped source and drain extensions, as schematically shown in Fig. 1(a). For the GNRFET, a wrapped-around gate is used as shown in Fig. 1(b). For the CNTFET, a coaxial gate is used as shown in Fig. 1(c). The nominal gate insulator is 3-nm-thick ZrO_2, which has a relative dielectric constant $\kappa \approx 25$. A power supply voltage of $V_{DD} = 0.5$ V is used.

The bandstructures of the CNT and GNR channels are required as an input to the transistor model. A nearest-neighbor p_z tight binding approach was used. The hopping integral was taken as t_{cc} = –2.7 eV. The edge effect plays an important role in the GNR, and a factor of 1.12 was used for the hopping parameter between two edge carbon atoms to take account of the edge relaxation effect [16]. For the AB-stacking structure of the multilayer graphene (Fig. 2), an interlayer coupling of 0.3 eV was set only for two vertically aligned atoms in two neighboring layers [17]. The nominal device has an interlayer coupling of zero, which is the lower limit of interlayer coupling. Weak interlayer coupling can be achieved by incommensurate non-AB-stacking, and leads to better device performance as discussed below. The nominal value was also varied in order to examine the effect of interlayer coupling strength on the device performance.

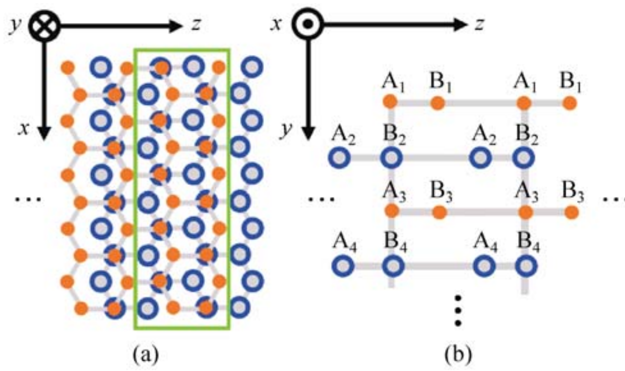

Figure 2 The atomistic structure of an AB-stacking multilayer GNR. The *z* direction is defined along the GNR transport direction, the *x* direction along the width direction, and the *y* direction along the thickness direction. "A" or "B" in (b) denotes atoms in A or B sublattices, respectively. The subscript denotes the layer index in a multilayer GNR. The modeled multilayer GNR has armchair edges

A "top-of-barrier" transistor model was used to assess the performance limits of the multilayer GNRFETs. The model fills the $+k$ states at the top of the barrier with the source Fermi level E_{FS} and the $-k$ states with the drain Fermi level E_{FD} as shown in Fig. 3(a). Self-consistent electrostatics was treated by a simple capacitance model, in which the gate insulator capacitance value was computed by a numerical Poisson solver and source- (drain-) channel capacitance was ignored for simplicity. The OP scattering in carbon nanotubes [18] or graphene nanoribbons has a short mean free path of ~10 nm, which could play an important role even for transistors with a sub-100 nm channel length. We also considered the transistor performance in the presence of OP scattering by setting an effective Fermi level at $E_F' = E_{ES} - \hbar\omega_{OP}$ which determines the population of the $-k$ states in the presence of OP scattering, as shown in Fig. 3(b). $\hbar\omega_{OP} \approx 0.18$ eV is the OP energy in CNTs and GNRs.

2. Results

Because the transistor performance strongly depends on the bandstructure of the channel material, we first examine the bandstructures of the multilayer GNRs. The upper left panel of Fig. 4(a) plots the bandstructure of the monolayer $n = 22$ AGNR, which has a width of $W_{GNR} \approx 2.7$ nm and a band gap of $E_g \approx 516$ meV. In contrast to a CNT in which a periodic boundary condition applies in the circumferential direction of the CNT and a valley degeneracy factor of two exists for each band, the monolayer AGNR does not have a valley degeneracy due to a different quantization boundary condition in the width direction of the GNR. At the limit of zero interlayer coupling, an m-layer GNR has the same bandstructure as the monolayer, but each band becomes m-fold degenerate due to the m uncoupled layers. The interlayer coupling lifts the subband degeneracy. Figure 4(a) also shows the bandstructures of two-, five-, and ten-layer multilayer GNRs with an AB stacking structure. As the number

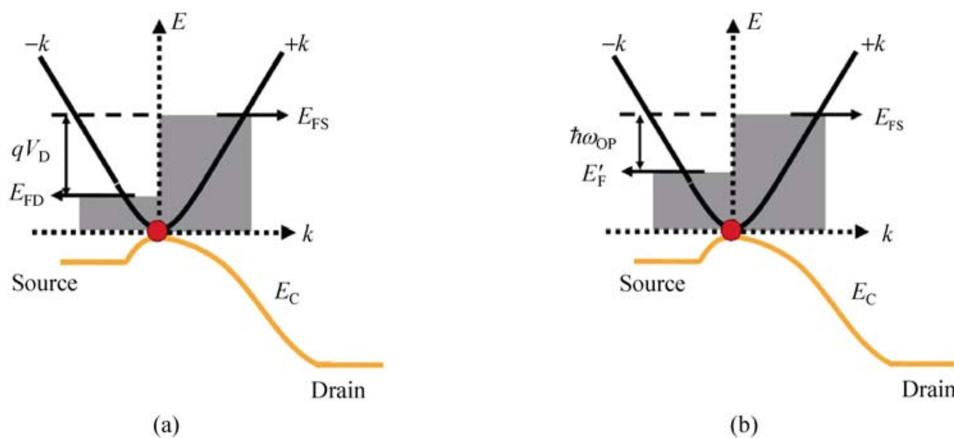

Figure 3 (a) In the "top of barrier" ballistic transistor model, the $+k$ states are filled according to the source Fermi level E_{FS}, and the $-k$ states are filled according to the drain Fermi level E_{FD}. (b) In the presence of OP scattering, the $-k$ states are filled according to an effective Fermi level, $E_F' = E_{FS} - \hbar\omega_{OP}$

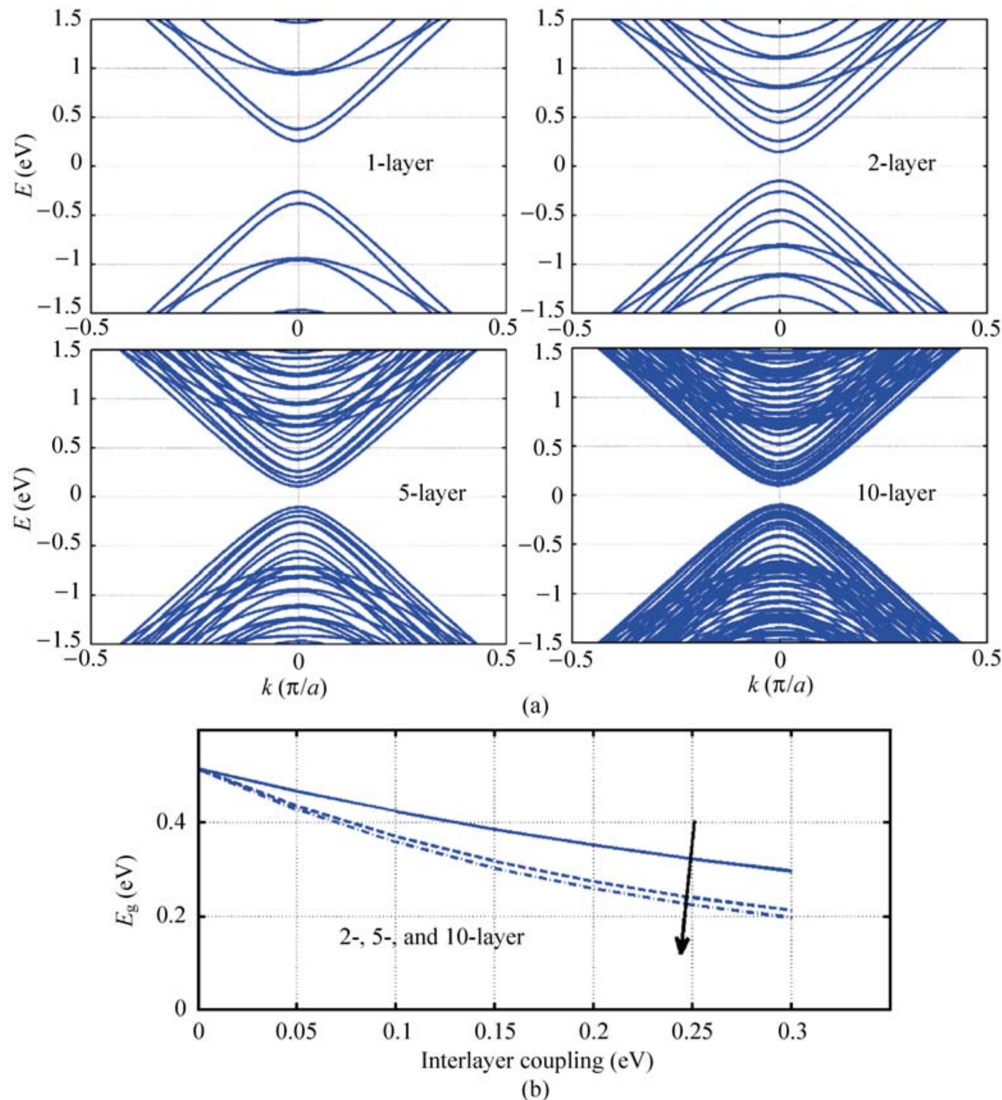

Figure 4 (a) The bandstructures of one-, two-, five-, and ten-layer $n = 22$ multilayer AGNRs with an interlayer coupling of 0.30 eV. The bandgap is 0.52 eV for one-layer, 0.30 eV for two-layer, 0.21 eV for five-layer, and 0.20 eV for ten-layer AGNRs. (b) The bandgap as a function of interlayer coupling for two-layer, five-layer and ten-layer $n = 22$ AGNRs

of layers increases, the subband spacing decreases, and the upper subbands should become more accessible for carrier transport. Furthermore, as the layer number increases from one to ten, the bandgap decreases from 516 meV to 197 meV. We also examined the dependence of the bandgap on the interlayer coupling strength for the multilayer GNRs as shown in Fig. 4(b). As the interlayer coupling strength increases from the zero limit to the value for the AB stacking structure, the bandgap decreases monotonically regardless of the number of GNR layers. The decrease is more significant for a multilayer GNR with a larger number of layers.

Next, we examine the effect of gating on transistor performance by varying the SiO_2 gate oxide thickness t_{ox} from 0.23 nm to 20 nm, as shown in Fig. 5. A common off-current of 10 nA was specified for all transistors. The lower limit of the simulated SiO_2 thickness is equivalent to the 3-nm-thick ZrO_2 gate for the modeled gating structure shown in Fig. 1, and results in the same gate insulator capacitance. The on-current increases only slightly by 12% as the number

of the layers increases from one to ten at $t_{ox} = 20$ nm as shown in Fig. 5(a). The transistor on-current is determined by the product of the charge density and the average carrier velocity at the top of the channel potential barrier. The relatively small improvement is largely due to a small increase in carrier density as the number of layers increases. The gate to channel capacitance C_g is a serial combination of insulator capacitance C_{ins} and the quantum capacitance C_q, and is limited by C_{ins} since C_{ins} is much smaller than C_q. A larger number of layers results in a slightly larger C_{ins} and thereby slightly larger C_g due to a thicker channel. For thick oxide gates, the advantage of using a multilayer GNR channel in terms of the on-current is insignificant.

In contrast, the advantage of the multilayer GNR channel in terms of the on-current becomes more significant as t_{ox} decreases, as shown in Fig. 5(a). Table 1 shows a comparison of the performance of various channels with a high-κ 3 nm ZrO_2. For a common off-current of 10 nA, the monolayer GNR channel has a slightly larger gate insulator capacitance, but a 13% smaller on-current than the CNT channel, because of the lack of valley degeneracy in the monolayer GNR. As the number of layers increases, the on-current surpasses that of the CNT. For a five-layer GNR, the on-current is 97% larger than that of the CNT, and for a ten-layer GNR, the on-current is 180% larger than that of the CNT. For a similar gating, the ballistic on-current of the multilayer GNR can be significantly larger than that of a CNT with a similar bandgap.

In order to understand the factors that contribute

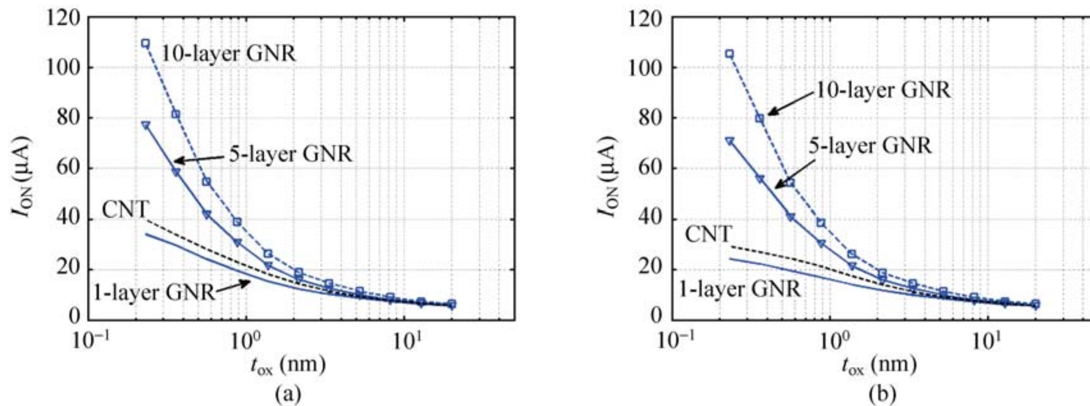

Figure 5 Effect of the gate insulator. The on-current as a function of the gate oxide thickness (a) at the ballistic limit and (b) in the presence of OP scattering for the GNRFETs and CNTFETs shown in Fig. 1. The one-, five-, and ten-layer $n = 22$ AGNRs with a zero interlayer coupling have a similar bandgap to the simulated (20, 0) CNT with a $E_{g,CNT} \approx 0.50$ eV to ensure a fair comparison. The gate insulator dielectric constant is $\kappa_{SiO_2} \approx 3.9$. The smallest simulated value of the oxide thickness, $t_{ox} \approx 0.23$ nm, is the equivalent value for a 3-nm thick ZrO_2 gate insulator with a dielectric constant of $\kappa \approx 25$, which results in the same gate insulator capacitance

Table 1 Comparison of the (20, 0) CNTFET with one-, five-, and ten-layer $n = 22$ GNRFETs at the ballistic performance limits. The transistor structures are shown in Fig. 1. The gate insulator thickness is 3 nm and the dielectric constant is 25 (for ZrO_2). The off-current (I_{OFF}), gate insulator capacitance (C_{ins}), on-current (I_{ON}), spacing between the source Fermi level and the top of the first subband barrier ($E_{FS} - E_1$), on-off current ratio (I_{ON}/I_{OFF}), and average carrier velocity at the top of the barrier ($\langle \upsilon(0) \rangle$) are compared. For the modeled one-layer GNR, the spacing between the first and second subbands is $E_2 - E_1 = 0.121$ eV. For the modeled CNT, $E_2 - E_1 = 0.226$ eV

	I_{OFF} (nA)	C_{ins} (F/m)	I_{ON} (μA)	$E_{FS} - E_1$ (eV)	I_{ON}/I_{OFF}	$\langle \upsilon(0) \rangle$ (cm/s)
CNT	10	8.42×10^{-10}	39.9	0.233	3900	4.28×10^{7}
One-layer GNR	10	8.98×10^{-10}	34.1	0.279	3400	4.61×10^{7}
Five-layer GNR	10	1.27×10^{-9}	77.3	0.155	7700	3.69×10^{7}
Ten-layer GNR	10	1.73×10^{-9}	109.6	0.120	11000	3.50×10^{7}

to the increase in the on-current, we also computed the gate insulator capacitance and the average carrier velocity as shown in Table 1. The average carrier velocity decreases from 4.28×10^7 cm/s to 3.50×10^7 cm/s as the number of GNR layers m increases from one to ten because more carriers populate closer to the bottom of the m-fold degenerate lowest subbands where the band-structure-limited velocity is low. The on-current, however, increases by a factor of 3.2 due to the increase in the gate capacitance C_g by a factor of 3.9. It is also interesting to note that the increase in the gate capacitance significantly outpaces the increase in the gate insulator capacitance stemming from a thicker GNR body as the number of GNR layers increases, because of the proportional increase in the quantum capacitance as a function of the number of the layers. Furthermore, for the modeled thin high-κ gate insulator, the quantum capacitance and the gate insulator capacitance become comparable, and both of them play a role in determining the gate capacitance.

The improvement in on-current is even more significant in the presence of OP scattering. As shown in Table 2, the on-current increases even more significantly as the number of layers increases in the presence of OP scattering. The on-current of the ten-layer GNR channel is 260% larger than that of the CNT. In addition, the average carrier velocity is also larger, which is different from the case of the ballistic channel as shown in Table 1. For a CNTFET, the OP scattering results in a saturation current close to $(4e^2/h)\times(\hbar\omega_{OP})\approx 28$ μA, where the OP energy $\hbar\omega_{OP}\approx$ 180 meV when only the first subband conducts the current, which is the case for the CNTFET because $E_{FS}-E_1\approx 216$ meV is smaller than the spacing between the first and second subbands $E_2-E_1\approx 226$ meV. The OP scattering results in considerably increased population of the –k states, which also lowers the average carrier velocity at the top of the barrier from 4.61×10^7 cm/s to 2.72×10^7 cm/s. In contrast, the effect of OP scattering on the ten-layer GNRFET is small, because the value of $E_{FS}-E_1\approx 120$ meV is smaller than the OP energy. In a multilayer GNR, more subbands are responsible for delivering the on-current, and therefore, the $E_{FS}-E_1$ value is smaller. As a result, the OP scattering only has a small effect on both the on-current and average carrier velocity of the ten-layer GNRFET. In constrast to the case of the ballistic channel, the average carrier velocity of the ten-layer GNRFET is also about 20% larger than that of the CNTFET in the presence of OP scattering, which promises faster intrinsic transistor speeds.

Finally, we examine the dependence of the on-current on the interlayer coupling. As shown in Fig. 6, the largest on-current is achieved at zero interlayer coupling and the on-current decreases as the interlayer coupling increases. The ballistic on-current monotonically decreases from 51 μA to 36 μA for two layers and from 77 μA to 58 μA for five layers as the interlayer coupling increases to the value for AB stacking. The reason is that an increase in the interlayer coupling increases the spacing between the subbands, which makes the higher subbands more difficult to be accessed for delivering the on-current. In addition, the increase in interlayer coupling also decreases the bandgap, as shown in Fig. 4. As the bandgap decreases, the band-to-band tunneling can be turned on, which can significantly increase the off-current. (Modeling the band-to-band tunneling current is beyond the capability of the semiclassical model used here.) Non-AB-stacking multilayer structures have been recently observed in experiments for both GNRs unzipped from CNTs [13] and CVD-grown multilayer graphene structures. Weakening the inter-layer coupling by non-AB-stacking, such as in randomly stacking structures, should be pursued in order to boost the performance of multilayer GNRFETs.

Table 2 The same comparison as Table 1 in the presence of OP scattering

With OP	I_{OFF} (nA)	C_{ins} (F/m)	I_{ON} (μA)	$E_{FS}-E_1$ (eV)	I_{ON}/I_{OFF}	$\langle\upsilon(0)\rangle$ (cm/s)
CNT	10	8.42×10^{-10}	29.3	0.216	2900	2.72×10^7
One-layer GNR	10	8.98×10^{-10}	24.4	0.260	2400	2.69×10^7
Five-layer GNR	10	1.27×10^{-9}	71.0	0.151	7100	3.30×10^7
Ten-layer GNR	10	1.73×10^{-9}	105.4	0.118	10500	3.33×10^7

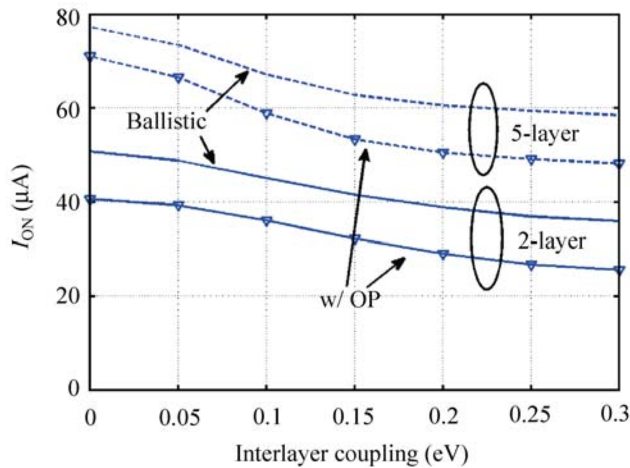

Figure 6 Effect of interlayer coupling. The on-current as a function of the interlayer coupling for the five-layer GNRFET (dashed lines) and the two-layer GNRFET (solid lines) as shown in Fig. 1. A 3-nm-thick ZrO_2 gate insulator is used. The lines without ▽ symbols are computed for a ballistic channel and the lines with ▽ symbols corrrespond to the presence of OP scattering

3. Discussions and conclusions

The performance of multilayer GNR MOSFETs can also be compared with that of silicon MOSFETs. Such a comparison is clouded by the different dimensionality of the channel material, and here we simply discuss how dense a GNR array channel needs to be to meet the performance goal at the end of the International Technology Roadmap for Semiconductors (ITRS roadmap) [19]. The ITRS roadmap calls for an on-current of about 2700 μA/μm and an off-current of 0.60 μA/μm at a power supply voltage of 0.65 V for the technology nodes near year 2020. To reach an on-current of 2700 μA/μm, a ten-layer array GNRFET with 26 GNRs per μm is needed as shown in Table 2. The array has an off-current of 0.26 μA/μm, which is less than half of the ITRS goal, although the power supply used in the GNRFET simulation is only 0.5 V. A recent experimental study characterized the mobility degradation of monolayer graphene on a SiO_2 substrate [20]. Another experimental study showed that a multilayer graphene transistor was more immune to noise compared with a monolayer graphene transistor [21], whose one-atom-thick body was susceptible to the charge impurities and oxide traps near the transistor channel. Therefore, the multilayer GNRFET is expected to have a better immunity to the adverse effects from substrates than the monolayer GNRFET.

The bandstructure of a multilayer GNR was assumed to be gate-voltage-independent in this study. Large electric fields and a significant potential drop between the layers, however, can alter the bandstructure of a multilayer GNR. For the simulated gate-all-around structure and a low applied voltage below 0.5 V, the electric field between the layers and the resulting potential drop between the layers is small (less than 30 meV as computed by a separate self-consistent atomistic simulation as described in Refs. [22, 23]). Its effect on the transistor *I*–*V* characteristics is negligible for the modeled gating structure and power supply voltage.

In summary, we have shown the important role of developing good gating technology and weakening the interlayer coupling in improving the performance of multilayer GNRFETs. The thin high-κ gate insulator is already in production for the Intel 45 nm transistor, but its application to GNRFETs remains to be developed. Weakening the interlayer coupling could be achieved experimentally in non-AB-stacking multi-layer graphene. The performance limits of a well-designed multilayer GNRFET can significantly exceed its CNT counterpart with a similar gate and bandgap in terms of the on-current, at either the ballistic limit or in the presence of OP scattering.

Acknowledgements

This work was supported by the National Science Foundation (NSF) and the Office of Naval Research (ONR), Intel, and MARCO MSD.

References

[1] Novoselov, K. S.; Geim, A. K.; Morozov, S. V.; Jiang, D.; Zhang, Y.; Dubonos, S. V.; Grigorieva, I. V.; Firsov, A. A. Electric field effect in atomically thin carbon films. *Science* **2004**, *306*, 666–669.

[2] Zhang, Y.; Tan, Y.; Stormer, H. L.; Kim, P. Experimental observation of the quantum Hall effect and Berry's phase in graphene. *Nature* **2005**, *438*, 201–204.

[3] Berger, C.; Song, Z.; Li, X.; Wu, X.; Brown, N.; Naud, C.; Mayou, D.; Li, T.; Hass, J.; Marchenkov, A. N.; Conrad, E. H.; First, P. N.; de Heer, W. A. Electronic confinement and coherence in patterned epitaxial graphene. *Science* **2006**, *312*, 1191–1196.

[4] Li, X.; Wang, X.; Zhang, L.; Lee, S.; Dai, H. Chemically derived, ultrasmooth graphene nanoribbon semiconductors. *Science* **2008**, *319*, 1229–1232.

[5] Lin, Y.; Perebeinos, V.; Chen, Z.; Avouris, P. Electrical observation of subband formation in graphene nanoribbons. *Phys. Rev. B* **2008**, *78*, 161409.

[6] Wang, X.; Ouyang, Y.; Li, X.; Wang, H.; Guo, J.; Dai, H. Room-temperature all-semiconducting sub-10-nm graphene nanoribbon field-effect transistors. *Phys. Rev. Lett.* **2008**, *100*, 206803.

[7] Ouyang, Y.; Wang, X.; Dai, H.; Guo, J. Carrier scattering in graphene nanoribbon field-effect transistors. *Appl. Phys. Lett.* **2008**, *92*, 243124.

[8] Gunlycke, D.; Lawler, H. M.; White, C. T. Room-temperature ballistic transport in narrow graphene strips. *Phys. Rev. B* **2007**, *75*, 085418.

[9] Ouyang, Y.; Yoon, Y.; Fodor, J. K.; Guo, J. Comparison of performance limits for carbon nanoribbon and carbon nanotube transistors. *Appl. Phys. Lett.* **2006**, *89*, 203107.

[10] Rahman, A.; Jing Guo; Datta, S.; Lundstrom, M. Theory of ballistic nanotransistors. *IEEE Trans. Electron Dev.* **2003**, *50*, 1853–1864.

[11] Chen, Z.; Appenzeller, J.; Knoch, J.; Lin, Y.; Avouris, P. The role of metal–nanotube contact in the performance of carbon nanotube field-effect transistors. *Nano Lett.* **2005**, *5*, 1497–1502.

[12] Javey, A.; Tu, R.; Farmer, D. B.; Guo, J.; Gordon, R. G.; Dai, H. High performance n-type carbon nanotube field-effect transistors with chemically doped contacts. *Nano Lett.* **2005**, *5*, 345–348.

[13] Jiao, L.; Zhang, L.; Wang, X.; Diankov, G.; Dai, H. Narrow graphene nanoribbons from carbon nanotubes. *Nature* **2009**, *458*, 877–880.

[14] Kosynkin, D. V.; Higginbotham, A. L.; Sinitskii, A.; Lomeda, J. R.; Dimiev, A.; Price, B. K.; Tour, J. M. Longitudinal unzipping of carbon nanotubes to form graphene nanoribbons. *Nature* **2009**, *458*, 872–876.

[15] Nakada, K.; Fujita, M.; Dresselhaus, G.; Dresselhaus, M. S. Edge state in graphene ribbons: Nanometer size effect and edge shape dependence. *Phys. Rev. B* **1996**, *54*, 17954.

[16] Son, Y.; Cohen, M. L.; Louie, S. G. Energy gaps in graphene nanoribbons. *Phys. Rev. Lett.* **2006**, *97*, 216803.

[17] Grüneis, A.; Attaccalite, C.; Wirtz, L.; Shiozawa, H.; Saito, R.; Pichler, T.; Rubio A. Tight-binding description of the quasiparticle dispersion of graphite and few-layer graphene. *Phys. Rev. B* **2008**, *78*, 205425.

[18] Yao, Z.; Kane, C. L.; Dekker, C. High-field electrical transport in single-wall carbon nanotubes. *Phys. Rev. Lett.* **2000**, *84*, 2941–2944.

[19] ITRS, International Technology Roadmap for Semiconductors, http://www.itrs.net (accessed oct 2, 2009).

[20] Chen, J.; Jang, C.; Xiao, S.; Ishigami, M.; Fuhrer, M. S. Intrinsic and extrinsic performance limits of graphene devices on SiO_2. *Nat. Nanotechnol.* **2008**, *3*, 206–209.

[21] Sui, Y.; Appenzeller, J. Screening and interlayer coupling in multilayer graphene field-effect transistors. *Nano Lett.* **2009**, *9*, 2973–2977.

[22] Guo, J.; Yoon, Y.; Ouyang, Y. Gate electrostatics and quantum capacitance of graphene nanoribbons. *Nano Lett.* **2007**, *7*, 1935–1940.

[23] Neophytou, N.; Paul, A.; Lundstrom, M.; Klimeck, G. Bandstructure effects in silicon nanowire electron transport. *IEEE Trans. Electron Dev.* **2008**, *55*, 1286–1297.